

Procedure for Estimating the Correlation Dimension of Optokinetic Nystagmus Signals

T. AASEN,* D. KUGIUMTZIS,† AND S. H. G. NORDAHL*

**Department of Otolaryngology/Head & Neck Surgery, Haukeland University Hospital, N-5021 Bergen, Norway; and †Department of Informatics, University of Oslo, P.O. Box 1080 Blindern, N-0316 Oslo, Norway*

Received April 23, 1995

In this study, optokinetic nystagmus (OKN) is hypothesized to be controlled by a low-dimensional deterministic and possibly chaotic generator. A procedure for quantifying the presumably low-dimensional structure of the OKN signal, based on the Singular Spectrum Approach and the Grassberger–Procaccia algorithm for estimating the correlation dimension, ν , is described. The procedure developed showed robustness against noise. Applying this method to OKN signals from 10 healthy subjects and 10 patients suffering from vertigo showed a statistically significant lower mean ν value for the patients. © 1997 Academic Press

1. INTRODUCTION

One of the tests used in the clinical evaluation of patients suffering from vertigo (dizziness) is the optokinetic test (1). Presented with a moving image, the eyes respond with a movement in the same direction as the image, interrupted by quick resetting phases. These reflexive, rhythmic eye movements, named optokinetic nystagmus (OKN), interact with the vestibulo-ocular reflex and the smooth pursuit function to hold objects steady on the retina. Despite this relatively simple function, the optokinetic nystagmus signal exhibits complicated behavior. Captured in the orbital cavity, the eyes bounce forth and back in a nonregular pattern (Fig. 1).

The mathematical ideas of deterministic, chaotic dynamics have introduced a new conceptual framework to understand and interpret dynamical phenomena. In medicine, where the complexity of physiological information processing often prevents us from making a reliable diagnostic evaluation, it is particularly interesting to see if the new tools in dynamical analysis can reveal information of clinical relevance.

To our knowledge, the first work in which nonlinear methods based on chaos theory were applied to OKN signals was published in 1992 by Shelhamer (2).

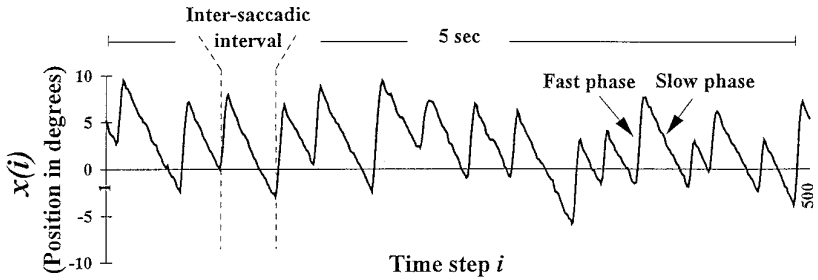


FIG. 1. Five-second registration of an optokinetic time series. Upward direction represents eye movement to the right, downward to the left. The optokinetic stimulation consists of vertical stripes moving with a constant velocity of $30^\circ/\text{sec}$ to the left.

He used the correlation dimension, ν , to detect nonlinear structure in the OKN signal, and he concluded that his procedure could evidently identify a chaotic underlying system. In 1990 and 1993, Aasen (3, 4) applied the same method to calorically induced nystagmus (bithermal water stimulation of the vestibular apparatus in the inner ear), and demonstrated that the underlying vestibular system can be described by a low-dimensional deterministic, possibly chaotic, system. Another study on calorically induced nystagmus (5) applied the correlation dimension parameter in order to discriminate between various vertigo types. The group of patients with normal test results (conventionally interpreted) and no detectable cause for their dizziness differed from the other groups by a statistically significant lower mean ν value. These preliminary reports motivated us to test whether the new analytic tools from the field of nonlinear dynamics can add some new information of clinical relevance. Before we reach this goal and hand the methods over to the clinicians, the methods must be thoroughly investigated.

In the present study it is hypothesized that nonregular optokinetic nystagmus behavior is due to nonlinear properties in the underlying physiological regulating system, and we focus on the correlation dimension estimate in order to characterize the presumable low-dimensional structure of the nystagmus attractor (cf. Section 3).

Based on the above considerations, our main goal was to find a standard procedure to compute the correlation dimension, i.e., choosing an appropriate method for the reconstruction of the state space with a certain parameter setting for the OKN signal (6, 7). Further, we wanted to see how the estimated dimension varied under different conditions of optokinetic stimulations.

In the next section, the recording specifications for the OKN signal are given. In Section 3, the state space reconstruction and the estimation of the correlation dimension are discussed. Finally, in Section 4, various aspects of applying the correlation dimension to OKN signals are considered and a procedure for the estimation is presented and applied to evaluate the OKN dynamics.

TABLE 1
THE DIFFERENT TYPES OF VERTIGO

Patient	Vertigo types
1.	Posttraumatic encephalopathy
2.	Barotrauma of the left ear
3.	Chronic otitis with fistula; reduced function of the left vestibular organ
4.	Progressive cerebellar atrophy with ataxia
5.	Acoustic neurinoma of the VIIIth cranial nerve on the right side
6.	Vestibular neuronitis, no sequela
7.	Other vestibular etiology
8.	Central etiology other than vascular
9.	Central vascular lesion
10.	Central vascular lesion

2. OPTOKINETIC TEST

2.1. Subjects

The OKN signals were recorded in 10 healthy subjects (mean age = 27 years, range 22 to 36) and 10 patients suffering from vertigo (mean age = 57 years, range 21 to 75). The patients diagnoses are given in Table 1.

2.2. Recording Technique

Horizontal eye movements were recorded with two electrodes (Ag–AgCl skin electrodes), placed laterally to each eye, and a reference electrode at the center of the forehead. The signal was amplified (10-sec time constant and an upper cutoff frequency of 30 Hz) and digitized into an IBM-compatible computer, using 12-bit A/D resolution and 100 Hz sampling frequency (sampling time $\tau_s = 0.01$).

2.3. Optokinetic Stimulation and Registration

Optokinetic nystagmus was obtained by stimulating the visual field with 3.75° width vertical light stripes separated by 11.25° width dark stripes. A slit projector presented the stripes on the inside of a hemispherical screen (100 cm in diameter). The subjects were sitting in front of the screen in a darkened room and were instructed not to follow the stripes with the eyes, but to focus their vision on the screen, allowing the optokinetic reflex to control the eye movements.

For the purpose of evaluating the response to different stimulation strengths, we used stripes moving with a velocity of 30 and 60°/sec, which are below and above the normal threshold for smooth pursuit function, respectively (8, 9). Four registrations were performed on each subject according to the direction and the velocity of the movement of the stripes: Left 30°/sec (L30), Right 30°/sec (R30), Left 60°/sec (L60), Right 60°/sec (R30). Between each test the subject was resting for a minimum of 60 sec in a darkened room.

3. METHODS

Our analyses make use of nonlinear methods based on chaos theory (the theory of deterministic systems with apparently random evolution due to sensitive dependence on small changes in the initial conditions (7)). In terms of chaos theory, geometrical objects formed by the system trajectories (so-called attractors) are characterized by fractal dimension. For attractors from regular deterministic systems, e.g., limit cycles or tori, the fractal dimension is equal to their topological dimension, but for attractors from chaotic systems (strange attractors) it is typically a noninteger that indicates their fractal structure. Among various measures of the fractal dimension the most common is the correlation dimension due to its computational simplicity (7, 10).

3.1. Grassberger–Procaccia’s Algorithm (GPA)

The correlation dimension ν is given by the scaling law

$$C(r) \propto r^\nu \quad [1]$$

for small r (11, 12). $C(r)$ is the correlation integral giving the probability of the interdistances of points on the attractor smaller than a radius r ,

$$C(r) = \frac{2}{N(N-1)} \sum_{i=1}^{N-1} \sum_{j=i+1}^N \theta(r - |\mathbf{x}_i - \mathbf{x}_j|), \quad [2]$$

and θ is the Heaviside function defined as $\theta(\rho) = 0$ for $\rho < 0$ and $\theta(\rho) = 1$ for $\rho \geq 0$ (for the definition of \mathbf{x} and N see Section 3.2.).

In practice, the correlation integral $C(r)$ is computed first, and then ν is estimated by the linear scaling between $\log C(r)$ and $\log r$ over a sufficient interval of r .

Certain parameters of GPA influence the estimation of ν and therefore must be adjusted properly. Neighbor points in state space that also are temporally close corrupt the computation of $C(r)$ (13). Therefore, points that are closer in time than some time limit corresponding to K data points are omitted from the calculations. The parameter K is called the “autocorrelation length.” The slope between $\log C(r)$ and $\log r$, which gives the estimated ν , can be computed either by linear regression or from the plateau of the first derivative of $\log C(r)$ over a scaling interval of distances $[r_1, r_2]$. Line fitting can always be applied, even when there is no real scaling. On the other hand, the derivative does not display a flat plateau unless the scaling is very clear. We prefer to estimate ν from the derivative of $\log C(r)$ and report the uncertainty by the standard deviation of the estimate.

To apply GPA to time series, a multidimensional state space from the scalar measurements is constructed first, and then the correlation integral is calculated for the reconstructed attractor.

3.2. Reconstruction of the State Space

Given a time series, an attractor can be embedded in a multidimensional state space. It is known that under certain conditions the reconstructed attractor preserves the topology of the original attractor of the system that generated the data (14–16). Working with OKN time series data from the vestibular system, the expression “the original attractor” refers to the interactivity of the global variables of the system. Carefully chosen reconstruction schemes are needed in order to maintain the equivalence of the two attractors.

In our work with OKN data, we have evaluated the two most common reconstruction methods, the *Method of Delays (MOD)* and the *Singular Spectrum Approach (SSA)*. For both methods, the chosen parameter setting is crucial for the estimation of v . In the following we shortly outline the two methods and their parameters; details can be found elsewhere (e.g., 17–20).

The sampled optokinetic nystagmus signal is denoted $\{x_{i\tau_s}\}_{i=1}^N = \{x(i\tau_s)\}_{i=1}^N$, where τ_s is the sampling time and N is the length of the time series.

3.2.1. Method of Delays. The reconstructed state vector with MOD is formed directly from the scalar measurements (21)

$$\mathbf{x}_i = [x_i, x_{i+\tau}, \dots, x_{i+(m-1)\tau}]^T, \quad [3]$$

where τ is the delay time, given as a multiple integer of the sampling time τ_s , and m is the embedding dimension of the reconstructed space. The parameters τ and m give the time window τ_w of length $(m-1)\tau$. The $N - (m-1)\tau \times m$ matrix

$$\mathbf{X} = [\mathbf{x}_1 \mathbf{x}_2 \dots \mathbf{x}_{N-(m-1)\tau}]^T \quad [4]$$

is then the constructed trajectory matrix.

The delay time τ is usually estimated as the value giving the least correlation among the components of \mathbf{x}_i . Linear decorrelation is obtained by choosing the first zero of the autocorrelation function $R(\tau)$ ($R(\tau_0) = 0$) or the correlation time τ_c corresponding to $R(\tau) = 1/e$, while general decorrelation is determined as the first local minimum of the mutual information function $I(\tau)$ ($\min I(\tau) = I(\tau_m)$) (22). However, these two functions often provide very large estimates of τ for the OKN time series, as shown in Fig. 2. This may result in a poor description of the details of the geometric shape of the attractor. In Fig. 3 we give illustrations of three MOD reconstructions of the OKN signal in R^2 with an arbitrary short delay time ($\tau = 8$), the minimum of $I(\tau)$, and the correlation time τ_c .

For the embedding dimension m , a lower limit for the reconstruction to be valid is given by Taken’s theorem, $m \geq 2d + 1$ (14). Taken originally proposed d to be the topological dimension, but recent theoretical results relax this criterion assigning d to the fractal dimension of the underlying attractor (16). In practice, however, lower values for m are often sufficient to reconstruct the attractor successfully, and one typically searches for the minimum embedding dimension m^* . A method often used to estimate m^* is the False Nearest Neighbors (FNN) (23). This method applies a geometrical criterion—based on the behavior of spatially near neighbors—to the attractor embedded in successively higher di-

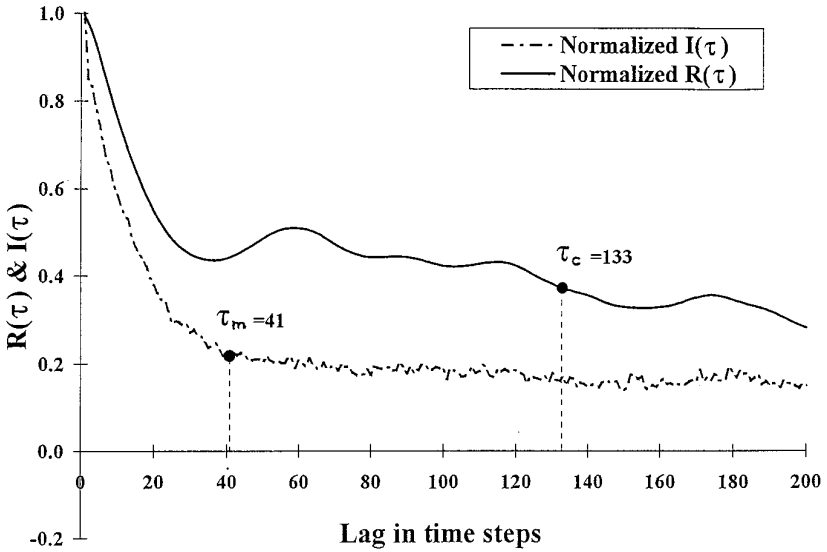


FIG. 2. The autocorrelation function $R(\tau)$ and mutual information function $I(\tau)$ of an optokinetic signal. Both $R(\tau)$ and $I(\tau)$ are normalized dividing with $R(0)$ and $I(0)$, respectively. The local minimum of $I(\tau)$, $\tau_m = 41$, and the autocorrelation time, $\tau_c = 133$, are marked. Note that the zero of $R(\tau)$ is not reached within this interval of lags.

mensions until a limit m^* is reached where the criterion is fulfilled. The implementation of this method to OKN data did not give unique m^* but showed a dependence of m^* on τ as shown in Fig. 4.

In the correlation dimension estimation with MOD reconstruction, only τ is the critical parameter since m is increased in order to investigate if there is a saturation of the scaling of $\log C(r)$ vs $\log r$.

3.2.2. Singular Spectrum Approach. Using SSA for the reconstruction, the state vector

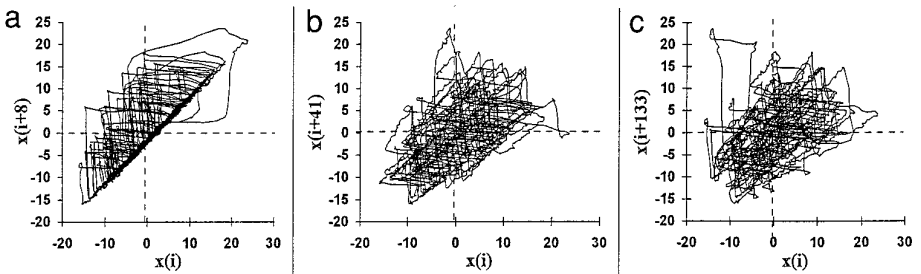


FIG. 3. Reconstructions of an optokinetic signal with MOD in R^2 and (a) $\tau = 8$, (b) $\tau = \tau_m = 41$, and (c) $\tau = \tau_c = 133$.

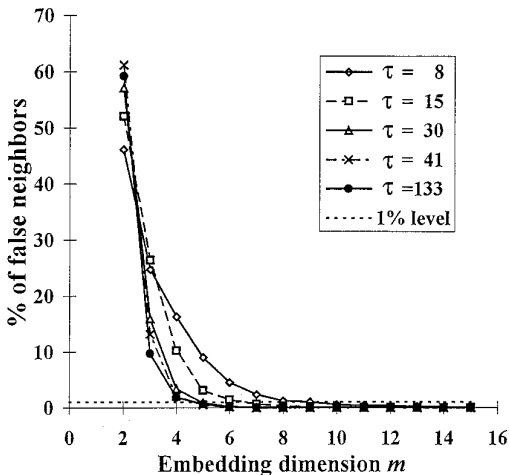


FIG. 4. The percentage of false nearest neighbors for increasing m . The 1% limit, often used as threshold level, is shown as a dashed horizontal line. The five lines correspond to reconstructions with MOD and $\tau = 8$, $\tau = 15$, $\tau = 30$, $\tau_m = 41$, and $\tau_c = 133$, giving different estimates of m^* .

$$\mathbf{x}_i = [x_i, x_{i+1}, \dots, x_{i+(p-1)}]^T \quad [5]$$

is formed for p large and $\tau = 1$, where the mean value of the time series is first subtracted from x_i . The trajectory in R^p is then the $(N - p + 1) \times p$ matrix

$$\mathbf{X} = [\mathbf{x}_1 \mathbf{x}_2 \cdots \mathbf{x}_{N-p+1}]^T. \quad [6]$$

A new basis for R^p is formed by the p singular vectors of \mathbf{X} computed with the Singular Value Decomposition (SVD) (17). The trajectory is then projected onto the m first singular vectors ranked according to the variance they explain, which correspond to the m largest singular values σ_i of \mathbf{X} . The final $(N - p + 1) \times m$ trajectory matrix is

$$\mathbf{Y} = [\mathbf{x}_1^T \mathbf{C} \mathbf{x}_2^T \mathbf{C} \cdots \mathbf{x}_{N-p+1}^T \mathbf{C}]^T, \quad [7]$$

where the $p \times m$ matrix \mathbf{C} has the m first singular vectors as columns.

The parameters of this method are the initial embedding dimension p and the final embedding dimension m . The initial embedding dimension p determines the time window length $\tau_w = (p - 1)$. For the estimation of m , the cutoff of the spectrum of singular values ($\sigma_1 > \cdots > \sigma_{m^*} \gg \sigma_{m^*+1} > \cdots > \sigma_p$) has been proposed, but for signals from nonlinear systems such a cutoff is not guaranteed (24).

Another approach to read m from the singular spectrum is to define a level of significance for the singular values. It is natural to choose it as the level of the noise floor, but this gives an undesirably large m^* unless the signal is very noise-corrupted. We believe that any general choice for m^* from the singular spectrum should be regarded as arbitrary in terms of nonlinear signal analysis,

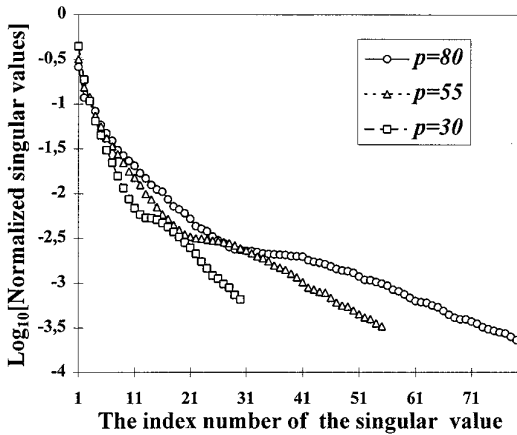


FIG. 5. The semilog plot of the normalized singular spectrum of an optokinetic signal (normalized by dividing with the first singular value). As shown in the figure the fall of the singular spectrum varies with p .

simply because the fall of the singular spectrum varies with p , as is shown for the OKN signal in Fig. 5.

Figure 6 illustrates the reconstructions with SSA of an OKN signal in R^3 and $p = 55$ (which is the mean intersaccadic interval; cf. Section 4). The three figures are the projections onto the planes formed by the three first singular vectors explaining about 60% of the variation of the data.

Based on an earlier study of one of us (20) we believe that the overall parameter for state space reconstruction (with MOD or SSA) is the time window length τ_w . In the next section, we validate these points when estimating the correlation dimension of the OKN signal.

4. THE ESTIMATION OF ν FOR OKN DATA

Concerning the parameter setting for GPA, we estimated ν from the plateau of the first derivative of $\log C(r)$ over the interval $[r_1, r_2]$ with $r_2/r_1 = 4$, choosing

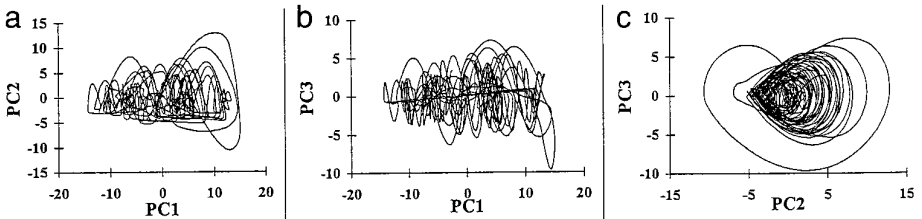


FIG. 6. Three 2-dimensional views of a 3-dimensional subspace formed by the combinations of the three first singular vectors, also called principal components (PC), of the reconstruction with SSA with initial embedding dimension $p = 55$: (a) PC1 and PC2, (b) PC1 and PC3, and (c) PC2 and PC3.

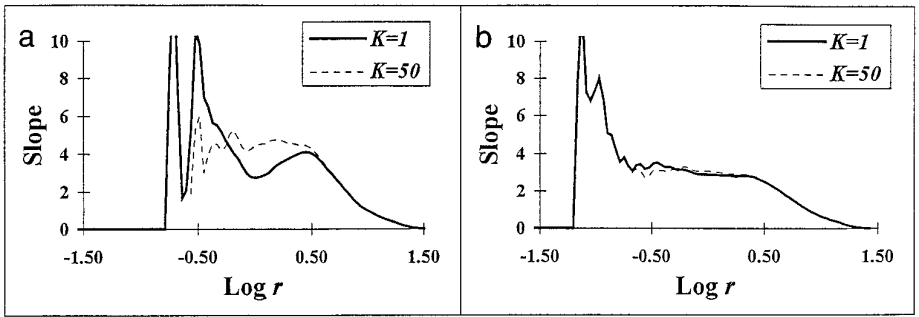


FIG. 7. The estimation of ν with autocorrelation length $K = 1$ and 50 for reconstructions with SSA ($m = 10$, $N = 6000$): (a) $p = 100$ results in too low estimate of ν for $K = 1$. (b) $p = 55$ gives no significant effect of K . (The same result is obtained using MOD.)

the interval that gives minimum standard deviation. An approximation to the derivative was performed by linear regression on each point and its two neighbors. Another parameter which turns out to be critical for the OKN data was the autocorrelation length K , as shown in Fig. 7 (13). In fact, the effect of K concerns only reconstructions with large τ_w . For larger τ_w the interdistances of points get larger and thus for small r values the time-correlated points affect critically the statistics of interdistances, giving a lower correlation dimension due to the colinear structure of these data points. The time scale where K starts to alter the estimated dimension is dependent on the sampling time τ_s . Faster sampling time increases the number of neighboring points in state space that also are temporarily close, and thus the K value has to be set higher in order to eliminate linear dependency.

We have applied the GPA method to reconstruct the OKN signal with both MOD and SSA. For MOD reconstructions, the estimation of ν varies with the parameter setting (Fig. 8). The saturation of the scaling area, if any, could only be observed for large τ_w , e.g., large m in combination with a large τ as in Fig. 8b. However, even when there was some sign of saturation, the scaling was very poor due to the embedding of a limited number of points in a high-dimensional space. This result is in agreement with similar work on other types of physiological data (25).

The application of the GPA to SSA reconstructions implies the computation of ν for the OKN data embedded in subspaces of R^p of successively higher m , where m varies from 2 to p . For each selection of p (which indicates the time window length, $\tau_w = p - 1$), saturation is always achieved. For some limit m' the curves for all $m \geq m'$ almost coincide because the variation of the attractor along the new directions (the $p - m'$ singular vectors) is negligible, and if τ_w is not very large a clear scaling is always observed (see Fig. 9). For τ_w larger than about three times the mean intersaccadic interval (see below), the scaling breaks down. However, we often observe a saturation of ν with a clear scaling region, i.e., with a relatively small standard deviation ($SD_{(r_2/r_1=4)}$) before the scaling

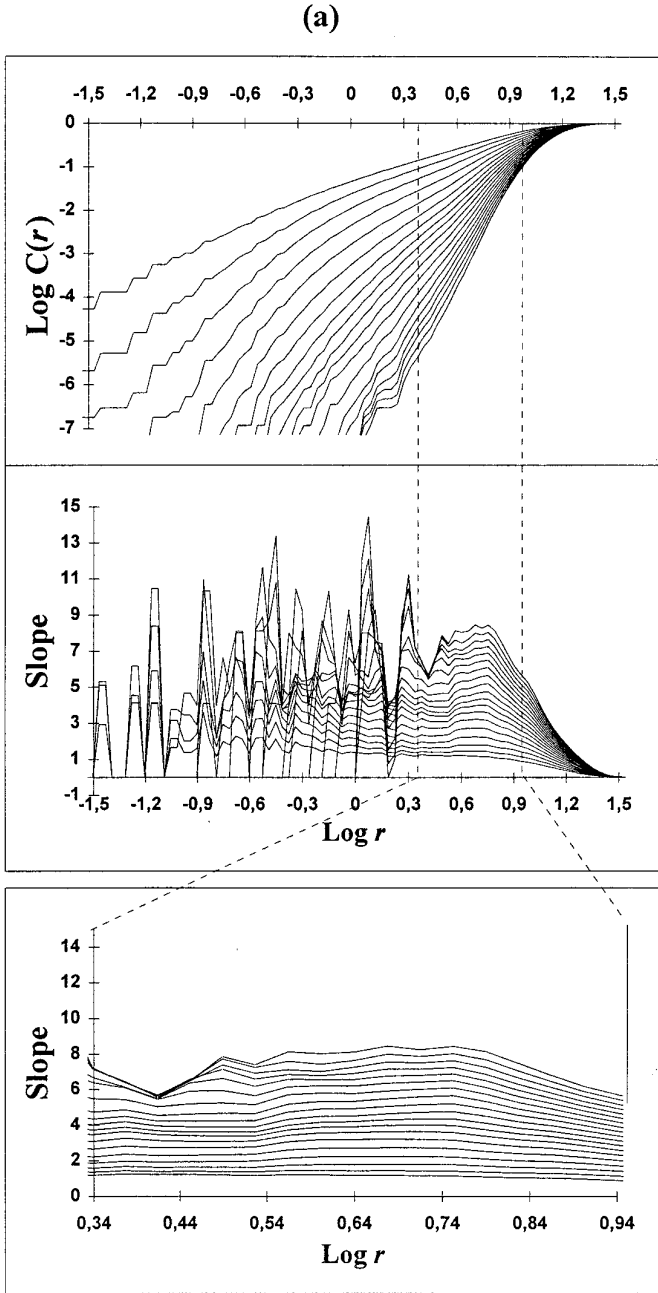


FIG. 8. Correlation integral $C(r)$ and the derivative (the slope between $\log C(r)$ and $\log r$) as a function of $\log r$. Reconstruction was done using MOD and $\tau = 8$ in (a) and $\tau = \tau_m = 41$ in (b). Embedding dimensions are plotted for $m = 2, \dots, 20$, i.e., $\tau_w = 8, 16, \dots, 152$ in (a) and $\tau_w = 41, 82, \dots, 779$ in (b). The graphs at the bottom focus on the scaling area $r_2/r_1 = 4$ with the smallest standard deviation for $m = 20$. The number of data points was $N = 6000$ for both (a) and (b).

(b)

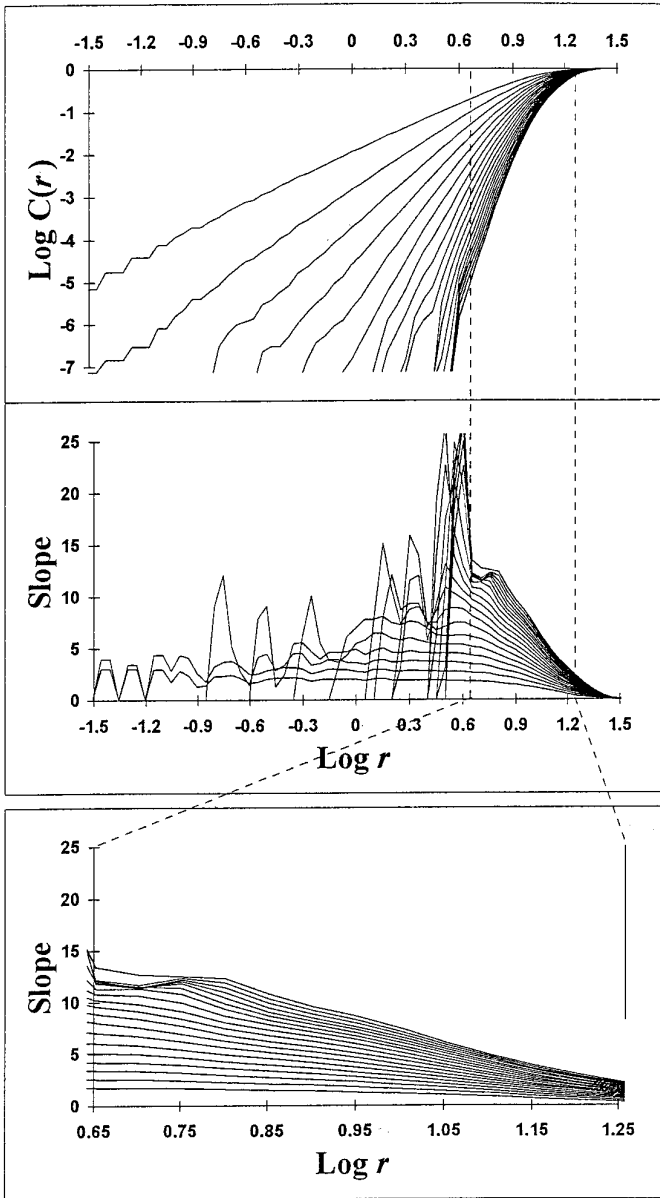


FIG. 8—Continued

(a)

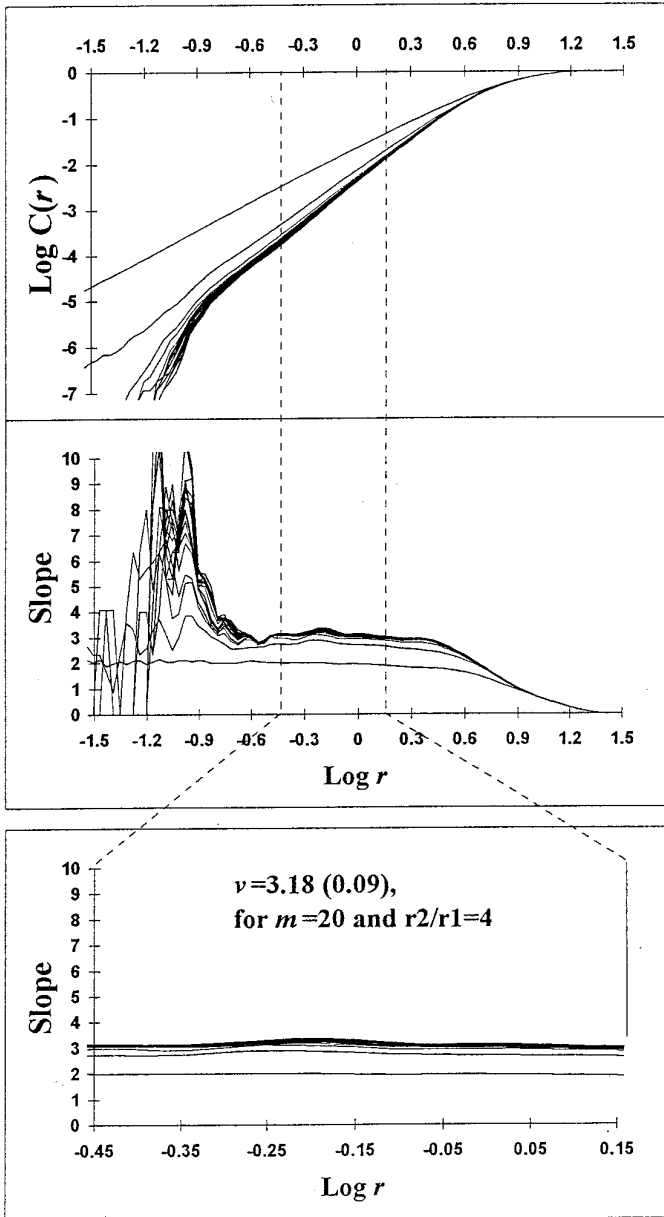


FIG. 9. Correlation integral $C(r)$ and the slope with SSA for $p = 55$ in (a) and $p = 165$ in (b). Embedding dimensions are plotted for $m = 2, \dots, 20$. The graphs at the bottom focus on the scaling area $r_2/r_1 = 4$ with the smallest standard deviation for $m = 20$. The number of data points was $N = 6000$ for both (a) and (b).

(b)

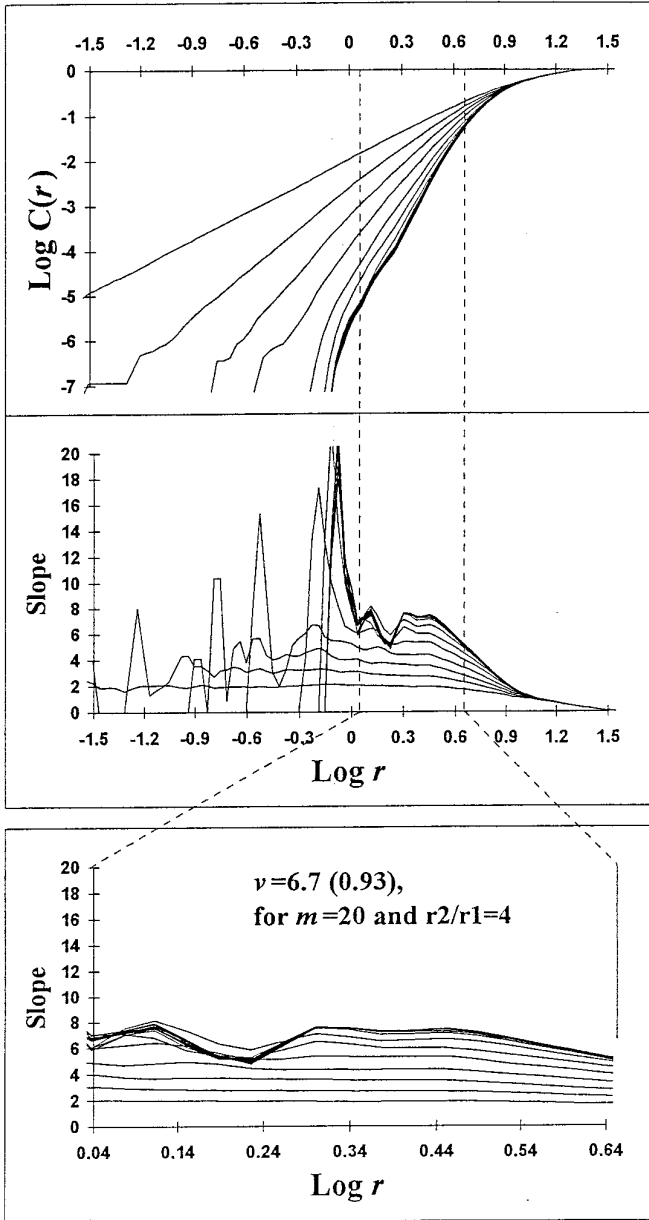


FIG. 9—Continued

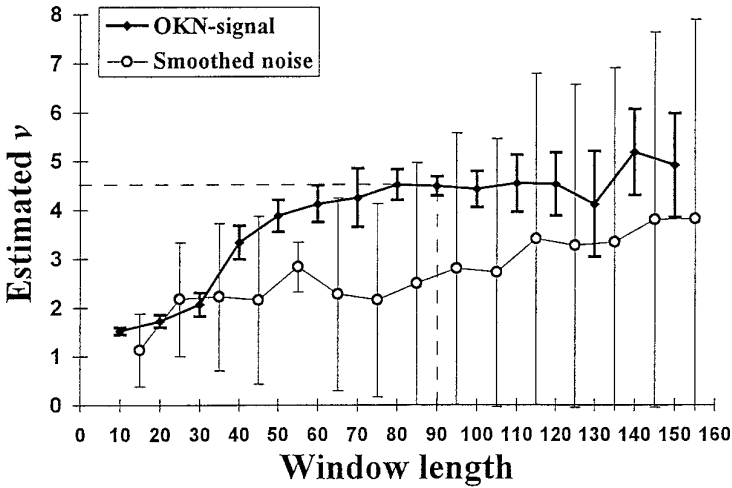


FIG. 10. The relation between the estimated ν (using SSA) and the windows length τ_w . A clear saturation of the ν value of about 4.5 is seen before the scaling breaks down. We also observe the lack of scaling area for a uniformed distributed noise signal smoothed with a 10-point moving average filter. The error bars show the standard deviation of the ν estimate in the interval $[r_1, r_2]$. For the optokinetic signal the p embedding dimension was projected onto the 10 most significant singular vectors ($m = 10$), which according to Fig. 9 totally defines the distribution of the points on the attractor. For the noise signal, m was set equal to p for $p \leq 45$. For $p > 45$, m was fixed to 45. The number of data points was $N = 6000$ for both signals.

collapses for larger τ_w , as shown in Fig. 10. Similar results are found when adding noise to data from simulated chaotic systems, e.g., Lorenz or Rössler (20). Applying the same procedure to a computer-generated smoothed noise-signal (Fig. 10) demonstrates the lack of scaling area for a random signal. A consequence of applying our automated procedure to random signals is an underestimation of ν , since the smallest $\text{SD}_{(r_2/r_1=4)}$ is found for large r , where the correlation integral saturates.

The method of surrogate data (26) provides further evidence of an underlying nonlinear structure in the reflexive eye movement signal, when constrained by optokinetic stimulation (Fig. 11). The surrogate data were generated by first transforming the original time series to the frequency domain using Fourier transform, randomizing the phases, and then transforming back to the time domain using inverse Fourier transform. The surrogate data generated as described above have the same linear correlations as the original, e.g., they have the same autocorrelation function. The differences in estimated ν values are therefore a result of nonlinearity in the data.

4.1. Which Reconstruction Method To Choose

The need to choose a standard procedure to derive estimates of ν is evident from the results using MOD and SSA reconstructions. When searching for nonlinear structures in OKN signals, it is desirable to eliminate redundant information

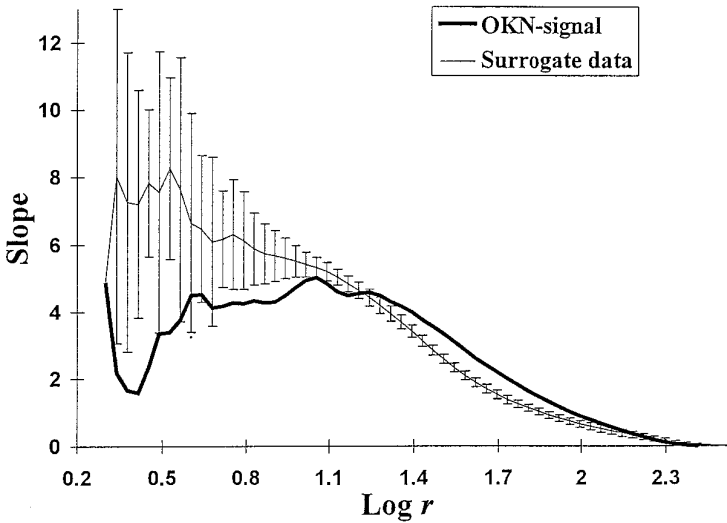


FIG. 11. The slope between $\log C(r)$ and $\log r$ for an OKN signal and for the mean and standard deviation of 20 surrogate data generated from the OKN-signal. For both the optokinetic signal and the surrogate data, $p = 90$ embedding dimension (see Fig. 10) was projected onto the 20 most significant singular vectors ($m = 20$). The number of data points was $N = 6000$.

about linear correlated patterns in the data. This is achieved with SSA which provides m linearly independent coordinates for any τ_w . Consequently, the signal-processing effect of SSA is an accentuation of the nonlinear structure in the signal. This is important when analyzing the OKN signal, which is highly dominated by slow phases (see Fig. 1) with approximately linear properties. The SSA reconstruction also serves as a built-in filter, ranking the coordinate axes according to the variance they explain in the data. To maintain linear independency with MOD, a large τ must be used, as emphasized by the decorrelation criteria, which results in an undesirably large τ_w , giving no clear scaling. Another advantage of using SSA is that once τ_w is chosen, the estimation of ν is straightforward, since the saturation for increasing m is guaranteed whenever the data show correlation.

The above considerations point out SSA as our choice.

4.2. Estimation Criterion

The estimation of ν requires that the linear scaling of $\log C(r)$ vs $\log r$ and the saturation of ν with increasing window length τ_w are within some limits. We applied the following procedure: For each initial embedding dimension p (corresponding to a τ_w), the pseudo-state space was projected onto the subspace spanned by the $m = 10$ largest singular vectors (see Fig. 10) and the slope was estimated in this subspace. The p was increased from $p = 10$, in increments of 10 ($p = 10, 20, 30, \dots$) until the difference between the maximum and minimum values of three successive slopes was below a predefined value. If this convergence

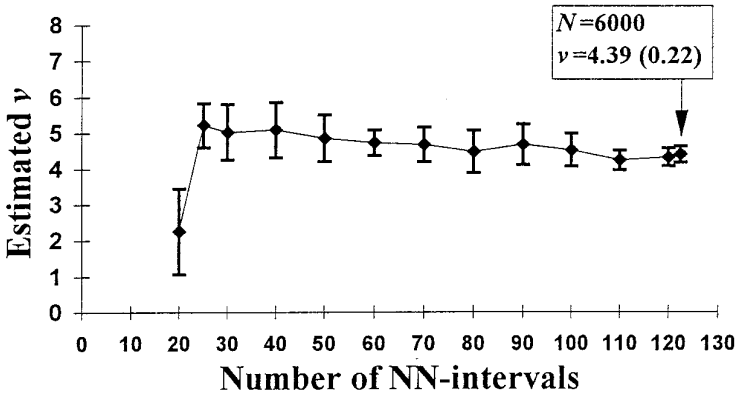


FIG. 12. The relation between the estimated correlation dimension ν and the time series length expressed in multiples of the mean intersaccadic interval. Reconstruction was done with SSA and the parameter setting $p = K = \tau_{NN} + 1 = 90$ and $m = 10$.

criterion was not reached for $p \leq 150$, a “not accepted” message was returned. Further, if the standard deviation¹ of the three accepted slopes was below a predefined level, the ν value was estimated to be the mean of the three slopes; otherwise, the not accepted message was returned.

4.3. The Time Series Length

Another important constraint in the computation of ν is the time series length, which should be long enough to represent clearly the reconstructed geometric object in state space. We evaluated the minimum OKN time series length in multiples of the intersaccadic interval, the so-called Nystagmus–Nystagmus interval (NN interval, τ_{NN}). The intersaccadic interval corresponds physiologically to the time intervals between the onset of consecutive fast components; functionally, it corresponds to the “smallest component” fulfilling the requirement of un-blurred vision (the eyes follow the image, interrupted by the fast resetting phase (the saccade)) and mathematically it corresponds to the dynamical excursion (the presumably fractal structure evolves from this “variations over the same theme”). Practically, τ_{NN} is simply the average of the time between maximums of the OKN time series, as shown in Fig. 1. To avoid false peaks due to noise, the data were filtered before the computation of τ_{NN} .

Figure 12 shows that the dimension does not change significantly after a time series length of approximately 60 τ_{NN} , which in the illustrated example is about 2000 data points ($\tau_{NN} = 32$). However, longer time series give more confident estimates.

Testing the hypothesis that the time series length necessary for estimating the

¹ This is the standard deviation of the plateau of the first derivative of $\log C(r)$ vs $\log r$ over the interval $[r_1, r_2]$ with $r_2/r_1 = 4$.

dimension is related to the number of NN intervals, and not directly to the number of data points (provided that the number of data points describing the NN interval reveal the overall geometric structure), we calculated the dimension for an OKN signal (cf. Fig. 10) using $\tau_s = 0.01, 0.02,$ and ≈ 0.03 (keeping every second and third data point) and the same window length τ_w ($p = 90, 45,$ and $30,$ respectively). For $\tau_s = 0.01$ ($n = 6000$) ν was estimated to 4.48 (0.2), for $\tau_s = 0.02$ ($n = 3000$) ν was 4.66 (0.39), and for $\tau_s \approx 0.03$ ($n = 2000$) we estimated $\nu = 4.64$ (0.47). Standard deviations are given in parentheses. Reducing the number of data points to the half and third while keeping the window length τ_w constant changed the estimated ν by only 0.18 and $0.16,$ respectively. This result supports the assumption that the information content of the OKN signal is related to the intersaccadic interval.

4.4. Filtering and Noise

To evaluate the robustness of the procedure, the estimates of ν for the OKN signals were compared to the estimates of the filtered OKN signals as well as the OKN signals corrupted with noise.

To smooth the signal, we used a standard low-pass FIR-filter of length 5 (cutoff frequency² of about 9 Hz, first zero crossing of the frequency response at 20 Hz) and a Savitzky and Golay (SG) 13-point cubic polynomial (27) (cutoff frequency of about 8 Hz, first zero crossing of the frequency response at 13 Hz).

To corrupt the OKN signal, Gaussian distributed noise with a SD of 5 and 10% the SD of the OKN signal was superimposed on the signal. It turned out that in the computation of the correlation integral, smoothing and noise affected only small interdistances, while the scaling was always observed in larger intervals of r as shown in Fig. 13. This is in contrast to earlier studies pointing out that linear filtering and adding noise to data can alter the estimated correlation dimension significantly (28). Our procedure applied to the OKN signal is robust to these changes.

4.5. Evaluating the OKN Dynamics

The procedure used for computing the correlation dimension of the OKN signals is summarized in the following steps:

Time series length: $N = 6000.$

- (1) Project the p ($p = 10, 20, . . .$) pseudo-state space onto the subspace defined by the first $m = 10$ singular vectors computed from the SVD of the trajectory matrix (m is larger than the number of the significant singular vectors).
- (2) Compute the correlation integral $C(r)$, setting the parameter of autocorrelation length K to $p = \tau_{NN} + 1.$
- (3) Estimate the slope between $\log C(r)$ and $\log r$ from the mean value of

² The cutoff frequency was defined by the -3 -dB level.

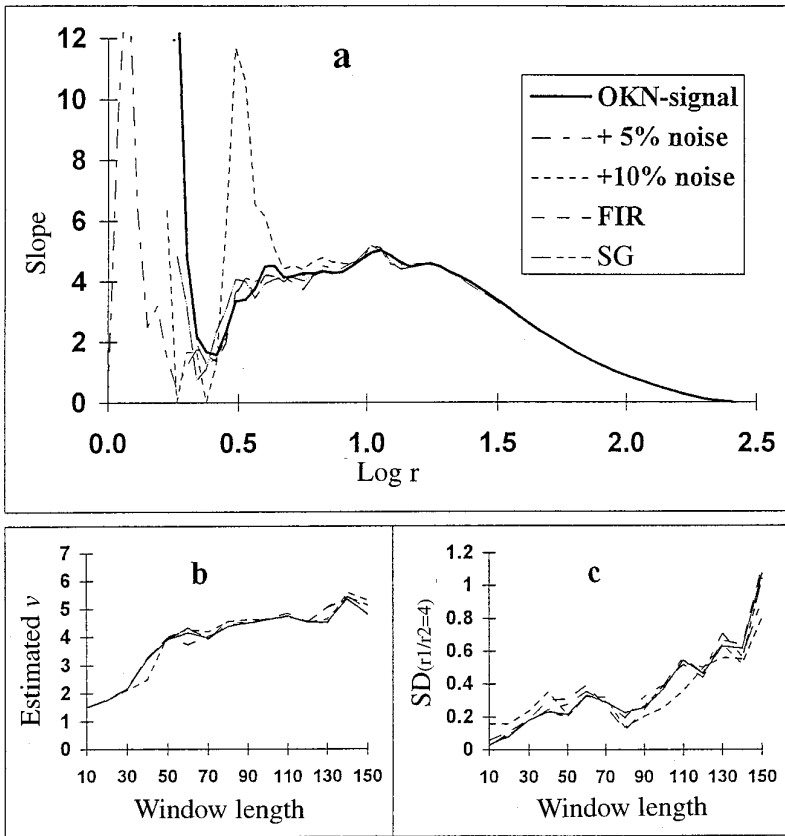


FIG. 13. (a) Estimation of ν for an optokinetic signal, for the optokinetic signal with superimposed noise, and for the smoothed optokinetic signal. Reconstruction was done with SSA and the parameter setting $p = K = 55$, $m = 10$ and $N = 6000$. (b, c) Estimated ν and $SD_{(r_1/r_2=4)}$ as a function of the time window length ($m = 10$ and $N = 6000$).

the first derivative of $\log C(r)$ over the scaling interval $r_2/r_1 = 4$ which gives the smallest standard deviation.

- (4) Repeat (1) to (3), increasing p in increments of 10, until the convergence and scaling criteria are obtained. The ν value is estimated as the mean of the last three computed slopes. If $p > 150$ is reached, a not accepted message is returned.

Testing for difference in the mean value of the estimated ν for the patients and the healthy subjects (applying the Student t test) for various combinations of the convergence and scaling criteria gave a statistically significant lower mean ν value for the patients (defined by a P value < 0.05) for a large section of parameter space (Fig. 14a). A convergence criterion of $\nu_{\max} - \nu_{\min} = 0.5$ and a scaling of $SD_{(r_2/r_1=4)} = 0.8$ gave, e.g., a P value of 0.018 [patients: mean = 4.35

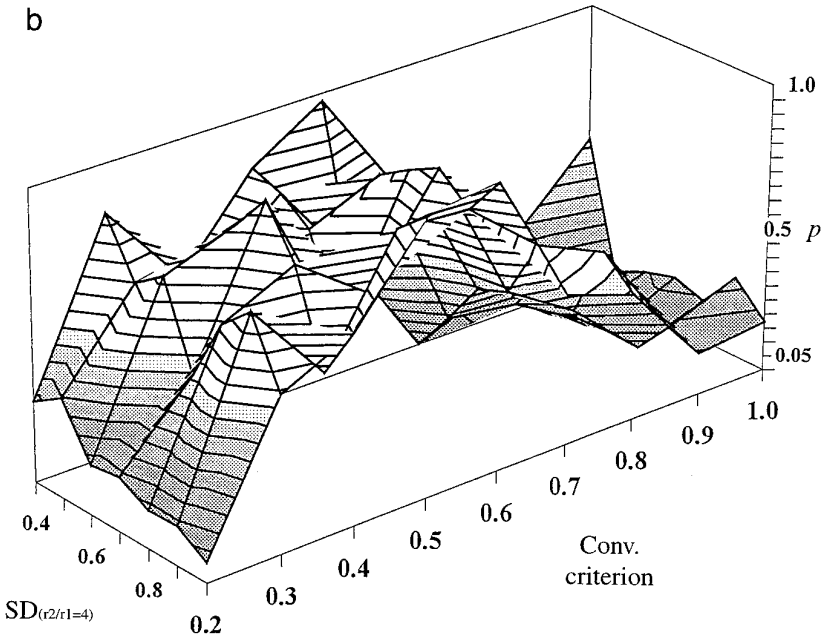
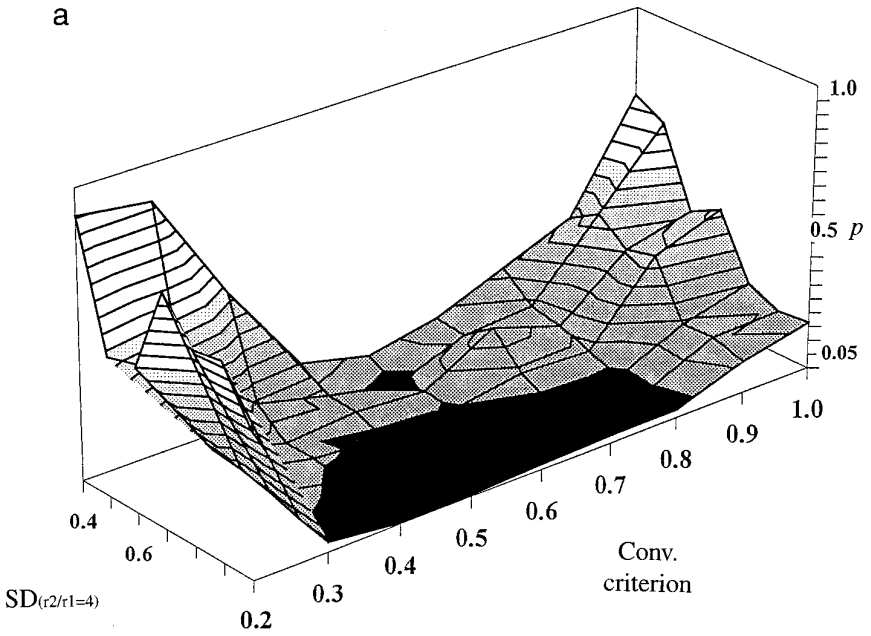


FIG. 14. (a) The vertical axis gives the P value from the statistical test (Student t test) of the difference in mean ν value between the group of vertigo patients and the healthy subjects, as a function of the convergence and scaling criterion. A large section of parameter space displays a P value below 0.05 (the dark area). (b) The same as (a), but here testing for difference between optokinetic stimulation below ($30^\circ/\text{sec}$) and above ($60^\circ/\text{sec}$) the threshold of smooth pursuit function. Statistical significance is not observed for any combinations of the convergence and scaling criterion.

(0.96), $n = 32$; healthy subjects: mean = 4.88 (0.71) $n = 28$; n is the number of accepted ν values of 40 registrations from each group according to Section 2]. A correlation coefficient of -0.12 and an estimated b parameter of -0.0066 from the fitted regression line to the correlation dimension, $\nu = a + bx$, where x is the age of the patients, indicates that the reported statistical significant difference between the two groups is not caused by the higher mean age in the group of patients. This result indicates a shift in the dynamics of the OKN generator for the patients, and it is likely that these disturbances of the underlying regulating mechanism also cause a reduced functionality of the balance system.

When we tested for difference between the response to optokinetic stimulation of 30 and 60°/sec, no such area appeared (Fig. 14b). We also randomly divided all 80 registrations (mixing both healthy subjects and patients) in two groups and generated the same surface plot. This was done 10 times, and all of the plots were comparable to Fig. 14b, with no area of significant P values.

5. DISCUSSION

The choice of SSA as the applied reconstruction method was based on practical considerations, mainly because it turned out to be a robust method. We do not claim that this technique is the most effective for extracting the dynamical properties of the OKN signal, or that the estimated ν value under the suggested procedure reveals the “true” dimensionality of the underlying physiological system. However, we believe that the ν value estimated here gives a measure of the variability of the signal, which reflects the interplay between the active components of the system, and thus is related to the global dimensionality.

Our aim was to find a robust procedure which gives a parameter that is related to the global dynamics of the vestibular system. A further step is to evaluate the possible clinical sensitivity of the method. This is of importance for the clinician who uses these signals for diagnostic purposes. The argument for possible clinical relevance can be put forward as follows: If the eye movement is pertinent to the vestibular system, and the pattern which falls within the window, τ_w , gives information of the state of the underlying physiological regulating system—which according to the applied method means that certain pathological conditions change the structure of the reconstructed nystagmus-attractor—then the correlation dimension, ν , can be regarded as a parameter of clinical relevance. In that case we will have a diagnostic tool comparable to, e.g., measuring the temperature of the body.

The fact that we find a statistically significant lower mean ν value for the group of vertigo patients compared to the healthy subjects could reflect a reduced functionality of the vestibular system in the vertigo group (e.g., a reduced ability to rapidly regulate and adapt to the ever-changing environment). The number of patients of each vertigo type was too small to establish any differences between them. Obviously, a study for evaluating the clinical validity of the method must include much larger groups with different vertigo types.

The fact that we did not find statistical difference between the average ν values to optokinetic stimulation above and in the range of smooth pursuit function³ indicates that it is the same underlying physiological regulating mechanism which is active under both conditions.

In contrast to Shelhamer (2) we found that the correlation dimension of the OKN signal is dependent on the time window τ_w .

6. CONCLUSION

The combination of the singular spectrum approach and the Grassberger–Procaccia algorithm for correlation dimension estimation fulfilled the requirement of a robust procedure, which could be used to evaluate the dynamics of the optokinetic nystagmus pattern. A statistically significant lower mean ν value in the group of vertigo patients compared to the healthy subjects was found.

It is not yet clear which qualities in the underlying physiological system the ν value reflects. Observing changes in the ν value according to various conditions (e.g., different levels of light intensity, different speed of the moving stripes) will give valuable information and point out relevant physiological correlates.

The procedure must be tested further for reliability (e.g., test–retest in a suitable population) and for possible clinical validity (e.g., the procedure applied to large representative groups with different vertigo types).

ACKNOWLEDGMENTS

We thank Professors Otto Inge Molvær (Haukeland University Hospital and Nuteq), Jan Olofsson (Haukeland University Hospital), and Nils Christophersen (University of Oslo) for helpful comments in the preparation of the manuscript. The study was partly supported by the Norwegian Research Council (D.K.).

REFERENCES

1. MAGNUSSON, M., SCHALÉN, L., PYYKKÖ, I., ENBOM, H., AND HENRIKSSON, N. G. Clinical considerations concerning horizontal optokinetic nystagmus. *Acta Otolaryngol. (Stockholm) Suppl.* **455**, 53 (1988).
2. SHELHAMER, M. Correlation dimension of optokinetic nystagmus as evidence of chaos in the oculomotor system. *IEEE Trans. Bio. Eng.* **39**, 1319 (1992).
3. AASEN, T. Analyse av vestibularisfunksjonen ved bruk av elektronystagmografi og moderne signalbehandlingsmetoder. Master's thesis, Rogaland University Center, Stavanger, Norway, 1990.
4. AASEN, T. Chaos theory applied to the caloric response of the vestibular system. *Comput. Biomed. Res.* **26**, 556 (1993).

³ Our analysis of optokinetic nystagmus above (60°/sec) and below (30°/sec) the limit of smooth pursuit was based on Ref. (8) (“Pursuit movements have . . . a maximum velocity of less than 50°/sec”) and Ref. (9) (“A target velocity of 40°/sec appears to be the limit for optimal functioning of the smooth pursuit system”). The reviewer has made us aware of a study (Meyer *et al.*, *Vision Res.* **25**, 561–563, 1985) which finds smooth pursuit movement up to 100°/sec. Our findings of no statistically significant difference between estimated ν values for optokinetic stimulation of 30 and 60°/sec is still valid, but according to Meyer *et al.* both conditions are within the range of smooth pursuit movement.

5. NORDAHL, S. H. G., AASEN, T., AND MOLVÆR, O. I. Fractal analysis of ENG-signals. Correlation dimension analysis. *Proc. Acta Otolaryngol. (Stockh)*, in press.
6. GRASSBERGER, P., SCHREIBER, T., AND SCHAFFRATH, C. Non-linear time sequence analysis. *Int. J. Bifurcation Chaos* **1**, 521 (1991).
7. KUGIUMTZIS, D., LILLEKJENDLIE, B., AND CHRISTOPHERSEN, N. Chaotic time series, part I: Estimation of some invariant properties in state space. *Modeling Ident. Control* **15**, 205 (1994).
8. SPALTON, D. J. Neuro-ophthalmology." In "Slide Atlas of Ophthalmology" (D. J. Spalton, R. A. Hitchings, and P. A. Hunter, Eds.). Gower Medical Publishing, 1984.
9. SCHALEN, L. Quantification of tracking eye movements in normal subjects. *Acta Otolaryngol. (Stock)* **90**, 404 (1980).
10. THEILER, J. Estimating fractal dimension. *J. Opt. Soc. Am. A* **7**, 1055 (1990).
11. GRASSBERGER, P., AND PROCACCIA, I. Characterization of strange attractors. *Phys. Rev. Lett.* **50**, 346 (1983).
12. GRASSBERGER, P., AND PROCACCIA, I. Measuring the strangeness of strange attractors. *Phys. D* **9**, 189 (1983).
13. THEILER, J. Spurious dimension from correlation algorithms applied to limited time-series data. *Phys. Rev. A* **34**, 2427 (1986).
14. TAKENS, F. Detecting strange attractors in turbulence. In "Dynamical Systems and Turbulence, Warwick 1980" (D. A. Rand and L. S. Young, Eds.), "Lecture Notes in Mathematics," Vol. 898, pp. 366–381. Springer, Berlin, 1981.
15. MAÑÉ, R. On the dimensions of the compact invariant sets of certain non-linear maps. In "Dynamical Systems and Turbulence, Warwick 1980" (D. A. Rand and L. S. Young, Eds.), "Lecture Notes in Mathematics," Vol. 898, pp. 230–242. Springer, Berlin, 1981.
16. SAUER, T., YORKE, J. A., AND CASDAGLI, M. Embedology. *J. Stat. Phys.* **65**, 579 (1991).
17. BROOMHEAD, D. S., AND KING, G. P. Extracting qualitative dynamics from experimental data. *Phys. D* **20**, 217 (1986).
18. ALBANO, A. M., MUENCH, J., SCHWARTZ, C., MEES, A. I., AND RAPP, P. E. Singular value decomposition and the grassberger-procaccia algorithm. *Phys. Rev. A* **38**, 3017 (1988).
19. CASDAGLI, M., EUBANK, S., FARMER, J. D., AND GIBSON, J. State space reconstruction in the presence of noise. *Phys. D* **51**, 52 (1991).
20. KUGIUMTZIS, D. State space reconstruction parameters in the analysis of chaotic time series—The role of the time window length. *Phys. D* **95**, 13 (1996).
21. PACKARD, N. H., CRUTCHFIELD, J. P., FARMER, J. D., AND SHAW, R. S. Geometry from a time series. *Phys. Rev. Lett.* **45**, 712 (1980).
22. FRASER, A. M., AND SWINNEY, H. Independent coordinates for strange attractors from mutual information. *Phys. Rev. A* **33**, 1134 (1986).
23. KENNEL, M. B., BROWN, R., AND ABARBANEL, H. D. I. Determining embedding dimension for phase-space reconstruction using a geometrical construction. *Phys. Rev. A* **45**, 3403 (1992).
24. MEES, A. I., RAPP, P. E., AND JENNINGS, L. S. Singular-value decomposition and embedding dimension. *Phys. Rev. A* **36**, 340 (1987).
25. BÉLAIR, J., GLASS, L., HEIDEN, U., AND MILTON, J. (Eds.) "Focus Issue: Dynamical Disease: Mathematical Analysis of Human Illness." *Chaos* **5**, 1995.
26. THEILER, J., EUBANK, S., LONGTIN, A., AND GALDRIKIAN, B. Testing for nonlinearity in time series: The method of surrogate data. *Phys. D* **58**, 77 (1992).
27. SAVITZKY, A., AND GOLAY, J. E. Smoothing and differentiation of data by simplified least squares procedure. *Anal. Chem.* **36**, 1627 (1964).
28. MITSCHKE, F., MOLLER, M., AND LANGE, W. Measuring filter chaotic signals. *Phys. Rev. A Gen. Phys.* **37**, 4518 (1988).